Inorganic Chemistry
Cite This: Inorg. Chem. 2019, 58, 8933−8937
Communication
pubs.acs.org/IC

Pressure-Induced Large Volume Collapse, Plane-to-Chain, Insulator to Metal Transition in $CaMn_2Bi_2$

Xin Gui,[†] Gregory J. Finkelstein,[‡] Keyu Chen,[§,∥] Tommy Yong,[‡] Przemyslaw Dera,[‡] Jinguang Cheng,*[,§,∥,⊥] and Weiwei Xie*[,†]

[†]Department of Chemistry, Louisiana State University, Baton Rouge, Louisiana 70803, United States
[‡]Hawai'i Institute of Geophysics and Planetology, University of Hawai'i at Manoa, Honolulu, Hawaii 96822, United States
[§]Beijing National Laboratory for Condensed Matter Physics and Institute of Physics, Chinese Academy of Sciences, Beijing, China 100190
[∥]School of Physical Sciences, University of Chinese Academy of Sciences, Beijing, China 100190
[⊥]Songshan Lake Materials Laboratory, Dongguan, Guangdong, China 523808

Supporting Information

ABSTRACT: In situ high pressure single crystal X-ray diffraction study reveals that the quantum material $CaMn_2Bi_2$ undergoes a unique plane to chain structural transition between 2 and 3 GPa, accompanied by a large volume collapse. Puckered Mn−Mn honeycomb layer converts to quasi-one-dimensional (1D) zigzag chains above the phase transition pressure. Single crystal measurements reveal that the pressure-induced structural transformation is accompanied by a dramatic 2 orders of magnitude drop of resistivity. Although the ambient pressure phase displays semiconducting behavior at low temperatures, metallic temperature dependent resistivity is observed for the high pressure phase, as surprisingly, are two resistivity anomalies with opposite pressure dependences, while one of them could be a magnetic transition and the other originates from Fermi surface instability. Assessment of the total energies for hypothetical magnetic structures for high pressure $CaMn_2Bi_2$ indicates that ferrimagnetism is thermodynamically favored.

The design and discovery of new quantum materials and advances in our ability to predict, detect, and exploit their properties will accelerate the development of future technologies.[1−3] In solid state quantum materials, conventional electronic and spin ordering can sometimes be broken down by quantum fluctuations, and consequently, entirely new forms of electronic or spin ordering can be observed.[4−6] Therefore, there is an urgent need to understand how to control and exploit electronic and spin interactions and quantum fluctuations in bulk materials with novel functionality. Initially, it was believed that quantum fluctuations can only be appreciable in magnetic materials where magnetic frustration is present;[7−11] however, it is now realized that strong spin−orbit coupling (SOC) can also produce the energies needed for quantum fluctuations.[12−14]

As the heaviest nonradioactive element, bismuth, in main group V, is located at the Zintl border in the periodic table.[15−20] Bi has moderate electronegativity (and can commonly act as either an anion or a cation) and strong spin−orbit coupling. Recent studies have shown that low dimensional materials with Bi layers are ideal platforms for realizing quantum topological electronic states, newly appreciated states of quantum matter.[21−23] The trigonal La_2O_3-type Mg_3Bi_2 has been proven to be an ideal platform for realizing type-II nodal line topological electronic states.[24] Usually, large magnetic moments on Mn^{2+} can cause extremely large d-band splitting between spin-up and spin-down (>7 eV), which drives the Mn d band far away from the Fermi level.[25] Some well-known intriguing behaviors in Mn-containing materials are giant magnetoresistance (GMR),[26,27] spin canting,[28] and metal−insulator transition (MIT),[29] and thus here we focus on a previously studied material, $CaMn_2Bi_2$, which displays both magnetism and strong spin−orbit coupling.[30,31] $CaMn_2Bi_2$ crystallizes in the same structure as Mg_3Bi_2, a trigonal La_2O_3-type structure with the $P\bar{3}m1$ space group at ambient pressure (*not* in the "usual" tetragonal 122 structure), in which layers of Mn and Bi are separated by Ca layers.[32] The Mn is in a bilayer that can be considered a puckered Mn honeycomb, which means that it has the potential to display unusual magnetically ordered states. The shortest Bi−Bi distance is ∼4.65 Å, and Mn resides in the center of the Bi_4 tetrahedron. Bi atoms may host possible topological electronic states and Mn@Bi_4 tetrahedron offers the platform for the interplay between magnetic moment from Mn and SOC effect from Bi.[33−35] The magnetic structure of ambient pressure $CaMn_2Bi_2$ obtained by neutron diffraction has shown that nearest-neighbor Mn atoms in the bilayer have opposing spins.[30] A common magnetic phenomenon associated with SOC is spin-canting, which has been observed and extensively investigated in various quantum systems such as $SrMnBi_2$ and $YbMnBi_2$.[36−38] Unfortunately, there is no direct evidence showing that spin-canting exists in $CaMn_2Bi_2$, suggesting that the interaction between SOC and magnetism is weak in this system at ambient pressure.

It is widely accepted that high pressure is the best tool for changing and controlling interatomic distances in solids—a fundamental property-determining parameter—because it

Received: May 9, 2019
Published: July 2, 2019

DOI: 10.1021/acs.inorgchem.9b01362
Inorg. Chem. 2019, 58, 8933−8937

cleanly changes such distances while not inducing structural disorder, which is the case for chemical pressure.[39−42] This tool has long been used, for example, to tune semiconductors, superconductors, and other solid-state materials to better understand their band structures and probe the electronic levels that arise from defects or impurities.[43−51] Pressure is particularly useful because the effects it induces are typically not associated with large changes in entropy, and therefore it frequently does not obscure subtle phase transitions. As a consequence, atomic and magnetic interaction parameters such as orbital energy and orbital overlap can be tuned and detected under pressure, and in the quantum material, $CaMn_2Bi_2$ may potentially enhance the interplay between SOC and magnetism.

First, we performed the study on crystal structures of $CaMn_2Bi_2$ under various pressures. According to the results of single crystal X-ray diffraction, up to 2.21 GPa $CaMn_2Bi_2$ adopts the same space group, $P\bar{3}m1$, as reported.[30] The diffraction patterns show that by compression to 3.56 GPa the sample has undergone a first order displacive phase transition and the space group changes to monoclinic $P2_1/m$. Due to the transformation mechanism, the sample retains its single crystal character. The detailed crystallographic data at various pressures are listed in Tables S1 and S2. In order to further characterize the material under pressure, we plot the curves of volume per formula unit vs pressure in Figure 1C and fit the

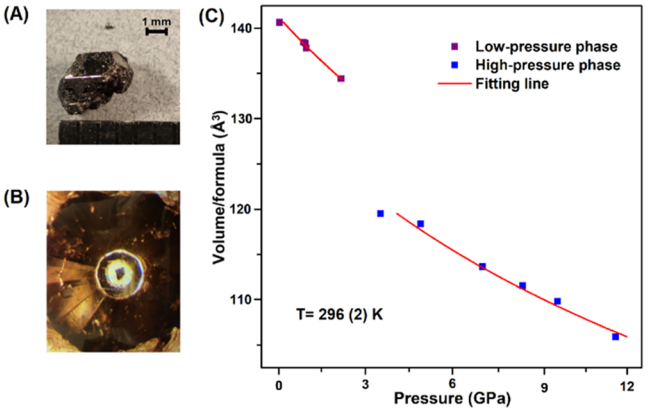

Figure 1. (A) $CaMn_2Bi_2$ single crystal. (B) Enlarged view of a Diamond Anvil Cell (DAC) filled with small $CaMn_2Bi_2$ single crystal and pressure medium. (C) Pressure dependence of the volume per formula unit of $CaMn_2Bi_2$.

data using the second-order Birch−Murnaghan equation of state, $P(V) = \frac{3B_0}{2}\left[\left(\frac{V_0}{V}\right)^{7/3} - \left(\frac{V_0}{V}\right)^{5/3}\right]$, where P is the pressure, V_0 is the reference volume, V is the deformed volume, and B_0 is the bulk modulus.[52] The phase transition is clearly visible in Figure 1C as a ∼7.5% discontinuity in the pressure dependence of the volume. The bulk moduli of low-pressure and high-pressure phases are fitted to be 38.6 (1.2) Pa and 36.1 (4.1) Pa, respectively. V_0 is fitted to be 131.4 (1.9) Å^3. Figure 2 shows both the low-pressure and high-pressure crystal structures of $CaMn_2Bi_2$. As can be seen in Figure 2A (left), the ambient-pressure phase consists of slightly distorted edge-shared Ca@Bi_6 octahedra with a tilting angle of only 0.24(2)° between Ca−Mn−Ca chains and the axis of regular octahedra, which increases to 0.36 (1)° at 0.99 GPa and 0.58(1)° at 2.21 GPa. In the low-pressure phase, the Mn atoms form a puckered

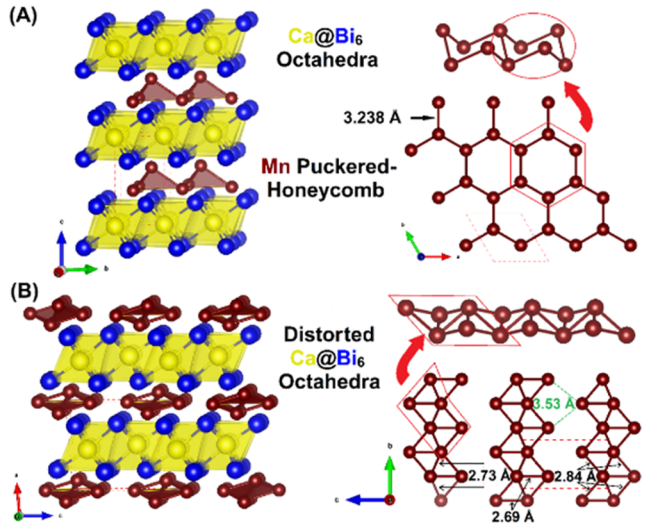

Figure 2. (A) Low-pressure structure of $CaMn_2Bi_2$ where yellow, brown, and blue balls represent Ca, Mn, and Bi atoms. (Left) Overview of the crystal structure consisting of edge-shared Ca@Bi_6 octahedra and Mn-puckered honeycomb. (Right) View on edge-shared Mn_6 ring in three-dimensional (3D) network. (B) Crystal structure of $CaMn_2Bi_2$ under high pressure. (Left) Crystal structure consisting with distorted edge-shared Ca@Bi_6 octahedra layers and distorted edge-shared Mn_6 chair conformation. (Right) View on distorted edge-shared Mn_6 ring in quasi-one-dimensional (quasi-1D) chain.

honeycomb when viewed down the *c*-axis (bottom right in Figure 2A). The high-pressure phase displays similar structural characteristics for the Ca@Bi_6 octahedra, except for the larger tilt angle and the Ca−Bi atomic distances. All Ca−Bi bond lengths at ambient pressure are 3.266 (1) Å while they range from 2.97(10) to 3.15(14) Å under 11.6 GPa. The Mn net, in contrast, exhibits distinct changes under high pressure (Figure 2B). Clearly, the Mn net rearranges from a puckered honeycomb to parallel one-dimensional (1D) zigzag ladder-like chains. The Mn−Mn separations in the ambient pressure phase are uniform at 3.238 Å, while the near-neighbor Mn−Mn distances within the change are much shorter, ranging from 2.69 (14) to 2.84 (10) Å in the monoclinic phase at 11.6 GPa. Importantly, the Mn−Mn distance between 1D chains is much longer, at 3.53(17) Å at 11.6 GPa.

We have also measured the high-pressure resistivity of two $CaMn_2Bi_2$ (samples #1 and #2) single crystals to verify the pressure-induced structural transformation and to characterize the electronic properties of the phases under pressure. Figure 3A displays the pressure dependence of the resistivity ($\rho(P)$) for these two samples measured between 0 and 3 GPa at room temperature. The resistivity of $CaMn_2Bi_2$ drops suddenly by 2 orders of magnitude at P_c = 2.15(5) and 2.35(5) GPa for samples #1 and #2, respectively, in good agreement with the structural phase transition detected by high-pressure single crystal XRD. The transition width of $\rho(P)$ around P_c is less than 0.1 GPa, reflecting good pressure homogeneity with the CAC and the dramatic nature of the phase transition. With difference observed in P_c in both samples, the one for sample #2 is more accurate, for which the reason is explained in the SI. The temperature-dependence of $\rho(T)$ from room temperature to 2 K at different pressures up to 7 GPa is shown in Figure 3B. At elevated temperatures ($T > T_N$), the curves exhibit "metallic" behavior originating from a strongly temperature-

DOI: 10.1021/acs.inorgchem.9b01362
Inorg. Chem. 2019, 58, 8933−8937

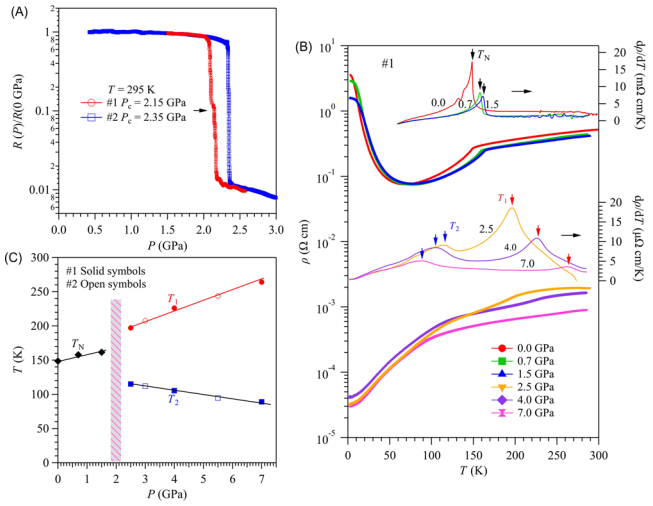

Figure 3. (A) Pressure dependence of resistivity for two $CaMn_2Bi_2$ single crystals (samples #1 and #2) at room temperature. (B)-Temperature dependence of resistivity $\rho(T)$ and its derivative $d\rho/dT$ under various pressures up to 7 GPa for a $CaMn_2Bi_2$ single crystal (sample #1). (C) Temperature−pressure phase diagram of the transitions in $CaMn_2Bi_2$ single crystals.

dependent mobility, which is not metallic, investigated by ref 40. The behavior below the structural phase transition at P_c has the same characteristics as observed at ambient pressure, with a kink anomaly at the antiferromagnetic transition $T_N \sim 150$ K, followed by an upturn at low temperatures. The transition temperature T_N can be defined clearly from the sharp peak in $d\rho/dT$ (Figure 3B). With increasing pressure, both T_N and the resistivity minimum gradually move to higher temperatures. Meanwhile, a resistivity plateau appears at low temperature and becomes more pronounced with increasing pressure. Given that the Mn−Mn interatomic distance decreases slightly with increasing pressure in the low-pressure phase, these results suggest that the antiferromagnetic interactions between the Mn localized moments, mediated by the conduction electrons, are strengthened upon the pressure-induced decrease of the interatomic distances. The results for sample #1 are given in Figure 3B on a semilogarithmic scale. Interestingly, $\rho(T)$ at $P > P_c$ displays some mild anomalies that vary systematically with pressure. For example, $\rho(T)$ at 2.5 GPa exhibits a kink-like anomaly at around 200 K followed by a shoulder-like anomaly centered around 116 K. These features can be described by a symmetric peak at T_1 and a broad hump at T_2 in the $d\rho/dT$ curve, as shown in the middle of Figure 3B. With increasing pressure, T_1 shifts quickly to higher temperatures while T_2 moves to lower temperatures, and the magnitudesof these anomalies in the $d\rho/dT$ curve are progressively suppressed. The insulator to metal transition can also be indexed by electronic calculations shown in Figures S3 and S4B.

Figure 3C illustrates the temperature−pressure phase diagram. The material undergoes its unique structural phase transition around $P_c \approx 2.35$ GPa, as described above. In the low-pressure trigonal phase, the antiferromagnetic transition temperature increases slightly under pressure. The high-pressure monoclinic phase, in contrast, is a metal that undergoes two phase transitions, at T_1 and T_2, which exhibit opposite pressure dependences within the pressure range investigated. Since the resistivity decreases with a larger slope at T_1 (Figures 3B and S1), it is likely that the transition at T_1 represents long-range magnetic order (the scattering rate for conduction electrons is reduced when magnetic moments are ordered). This is supported by the fact that the positive pressure effect for T_1 is similar to that seen for T_N in the low-pressure phase. In contrast, the broad hump feature around T_2 may be associated with the formation of a spin or charge density wave phase, which can be suppressed by pressure. This scenario is consistent with the chain-based quasi-1D structure and enhanced electrical conductivity in the high-pressure phase. Further neutron diffraction study would be of interest to determine the origin of these transitions in high-pressure chain-based $CaMn_2Bi_2$.

In summary, $CaMn_2Bi_2$ undergoes a structural phase transition from puckered Mn−Mn honeycomb layer to quasi-1D Mn−Mn chains at $P_c \approx 2.35$ GPa. The high-pressure resistivity measurements show two electronic transitions with opposite temperature dependence while one of them can be seen as antiferromagnetic ordering transition and the other is speculated to originate from the instability from Fermi surface, which is proven by the LMTO calculations.

■ ASSOCIATED CONTENT

Supporting Information

The Supporting Information is available free of charge on the ACS Publications website at DOI: 10.1021/acs.inorgchem.9b01362.

Sample Preparation; Single Crystal Structure Determination and Analysis at Various Pressures; Electrical Measurements at Various Pressures; Electronic Structural Calculations and Analysis (PDF)

Accession Codes

CCDC 1916519 and 1916930 contain the supplementary crystallographic data for this paper. These data can be obtained free of charge via www.ccdc.cam.ac.uk/data_request/cif, or by emailing data_request@ccdc.cam.ac.uk, or by contacting The Cambridge Crystallographic Data Centre, 12 Union Road, Cambridge CB2 1EZ, UK; fax: +44 1223 336033.

■ AUTHOR INFORMATION

Corresponding Authors

*E-mail: jgcheng@iphy.ac.cn.
*E-mail: weiweix@lsu.edu.

ORCID

Jinguang Cheng: 0000-0002-4969-1960
Weiwei Xie: 0000-0002-5500-8195

Notes

The authors declare no competing financial interest.

■ ACKNOWLEDGMENTS

The work at LSU was supported by the U.S. Department of Energy, Office of Science, Basic Energy Sciences, under EPSCoR Grant No. DE-SC0012432 with additional support from the Louisiana Board of Regents. Authors deeply appreciate technical support from Louisiana State University-Shared Institute Facility (SIF) for SEM-EDS. G.F. and P.D. acknowledge support from the University of Hawaii Materials Science Consortium for Research and Education (MSCoRE). JGC is supported by the National Key R&D Program of China (2018YFA0305702), the National Natural Science Foundation of China (11574377, 11834016, and 11874400), the Strategic Priority Research Program and Key Research Program of

DOI: 10.1021/acs.inorgchem.9b01362
Inorg. Chem. 2019, 58, 8933−8937

Frontier Sciences of the Chinese Academy of Sciences (XDB25000000 and QYZDB-SSW-SLH013).

REFERENCES

(1) Mohseni, M.; Rebentrost, P.; Lloyd, S.; Aspuru-Guzik, A. Environment-Assisted Quantum Walks in Photosynthetic Energy Transfer. *J. Chem. Phys.* **2008**, *129*, 174106.

(2) Moore, J. E. The Birth of Topological Insulators. *Nature* **2010**, *464*, 194−198.

(3) Aspuru-Guzik, A.; Walther, P. Photonic Quantum Simulators. *Nat. Phys.* **2012**, *8*, 285−291.

(4) Mukhanov, V. F.; Chibisov, G. V. Quantum Fluctuations and a Nonsingular Universe. *JETP Lett.* **1981**, *33*, 532−535.

(5) Peano, V.; Houde, M.; Marquardt, F.; Clerk, A. A. Topological Quantum Fluctuations and Traveling Wave Amplifiers. *Phys. Rev. X* **2016**, *6*, 041026.

(6) Laflorencie, N. Quantum Entanglement in Condensed Matter Systems. *Phys. Rep.* **2016**, *646*, 1−59.

(7) Balents, L. Spin Liquids in Frustrated Magnets. *Nature* **2010**, *464*, 199−208.

(8) Lee, P. A. 40 Years of Quantum Spin Liquid: A Tale of Emergence from Frustration. In *PWA90: A Lifetime of Emergence*; WORLD SCIENTIFIC, 2015; pp 105−111.

(9) Yao, N. Y.; Zaletel, M. P.; Stamper-Kurn, D. M.; Vishwanath, A. A Quantum Dipolar Spin Liquid. *Nat. Phys.* **2018**, *14*, 405.

(10) Zhou, Y.; Kanoda, K.; Ng, T.-K. Quantum Spin Liquid States. *Rev. Mod. Phys.* **2017**, *89*, 025003.

(11) Law, K. T.; Lee, P. A. 1T-TaS_2 as a Quantum Spin Liquid. *Proc. Natl. Acad. Sci. U. S. A.* **2017**, *114*, 6996−7000.

(12) Christensen, M. H.; Orth, P. P.; Andersen, B. M.; Fernandes, R. M. Emergent Magnetic Degeneracy in Iron Pnictides Due to the Interplay between Spin-Orbit Coupling and Quantum Fluctuations. *Phys. Rev. Lett.* **2018**, *121*, 057001.

(13) Banerjee, A.; Bridges, C. A.; Yan, J.-Q.; Aczel, A. A.; Li, L.; Stone, M. B.; Granroth, G. E.; Lumsden, M. D.; Yiu, Y.; Knolle, J.; Bhattacharjee, S.; Kovrizhin, D. L.; Moessner, R.; Tennant, D. A.; Mandrus, D. G.; Nagler, S. E. Proximate Kitaev Quantum Spin Liquid Behaviour in a Honeycomb Magnet. *Nat. Mater.* **2016**, *15*, 733−740.

(14) Nam, H.; Chen, H.; Liu, T.; Kim, J.; Zhang, C.; Yong, J.; Lemberger, T. R.; Kratz, P. A.; Kirtley, J. R.; Moler, K.; Adams, P. W.; MacDonald, A. H.; Shih, C.-K. Ultrathin Two-Dimensional Superconductivity with Strong Spin−Orbit Coupling. *Proc. Natl. Acad. Sci. U. S. A.* **2016**, *113*, 10513−10517.

(15) Fässler, T. F.; Hoffmann, S. D. Endohedral Zintl Ions: Intermetalloid Clusters. *Angew. Chem., Int. Ed.* **2004**, *43*, 6242−6247.

(16) Saparov, B.; Bobev, S. Isolated $_\infty^1[ZnPn_2]^{4-}$ Chains in the Zintl Phases Ba_2ZnPn_2 (Pn = As, Sb, Bi)-Synthesis, Structure, and Bonding. *Inorg. Chem.* **2010**, *49*, 5173−5179.

(17) Gascoin, F.; Ottensmann, S.; Stark, D.; Haïle, S. M.; Snyder, G. J. Zintl Phases as Thermoelectric Materials: Tuned Transport Properties of the Compounds $Ca_xYb_{1-x}Zn_2Sb_2$. *Adv. Funct. Mater.* **2005**, *15*, 1860−1864.

(18) Chan, J. Y.; Kauzlarich, S. M.; Klavins, P.; Shelton, R. N.; Webb, D. J. Colossal Magnetoresistance in the Transition-Metal Zintl Compound $Eu_{14}MnSb_{11}$. *Chem. Mater.* **1997**, *9*, 3132−3135.

(19) Chan, J. Y.; Wang, M. E.; Rehr, A.; Kauzlarich, S. M.; Webb, D. J. Synthesis, Structure, and Magnetic Properties of the Rare-Earth Zintl Compounds $Eu_{14}MnPn_{11}$ and $Eu_{14}InPn_{11}$ (Pn = Sb, Bi). *Chem. Mater.* **1997**, *9*, 2131−2138.

(20) Corbett, J. D. Polyanionic Clusters and Networks of the Early P-Element Metals in the Solid State: Beyond the Zintl Boundary. *Angew. Chem., Int. Ed.* **2000**, *39*, 670−690.

(21) Hor, Y. S.; Williams, A. J.; Checkelsky, J. G.; Roushan, P.; Seo, J.; Xu, Q.; Zandbergen, H. W.; Yazdani, A.; Ong, N. P.; Cava, R. J. Superconductivity in $Cu_xBi_2Se_3$ and Its Implications for Pairing in the Undoped Topological Insulator. *Phys. Rev. Lett.* **2010**, *104*, 057001.

(22) Qu, D.-X.; Hor, Y. S.; Xiong, J.; Cava, R. J.; Ong, N. P. Quantum Oscillations and Hall Anomaly of Surface States in the Topological Insulator Bi_2Te_3. *Science* **2010**, *329*, 821−824.

(23) Haazen, P. P. J.; Laloë, J.-B.; Nummy, T. J.; Swagten, H. J. M.; Jarillo-Herrero, P.; Heiman, D.; Moodera, J. S. Ferromagnetism in Thin-Film Cr-Doped Topological Insulator Bi_2Se_3. *Appl. Phys. Lett.* **2012**, *100*, 082404.

(24) Chang, T. R.; Pletikosic, I.; Kong, T.; Bian, G.; Huang, A.; Denlinger, J.; Kushwaha, S. K.; Sinkovic, B.; Jeng, H. T.; Valla, T.; Xie, W.; Cava, R. J. Realization of a Type-II Nodal-Line Semimetal in Mg_3Bi_2. *Adv. Sci.* **2019**, *6*, 1800897.

(25) Li, J.; Wang, C.; Zhang, Z.; Gu, B. L.; Duan, W.; Xu, Y. Magnetically Controllable Topological Quantum Phase Transitions in Antiferromagnetic Topological Insulator $MnBi_2Te_4$; *arXiv:1905.00642*, **2019**.

(26) Jin, S.; Tiefel, T. H.; McCormack, M.; Fastnacht, R. A.; Ramesh, R.; Chen, L. H. Thousandfold Change in Resistivity in Magnetoresistive La-Ca-Mn-O Films. *Science* **1994**, *264*, 413−415.

(27) Subramanian, M. A.; Toby, B. H.; Ramirez, A. P.; Marshall, W. J.; Sleight, A. W.; Kwei, G. H. Colossal Magnetoresistance without Mn^{3+}/Mn^{4+} Double Exchange in the Stoichiometric Pyrochlore $Tl_2Mn_2O_7$. *Science* **1996**, *273*, 81−84.

(28) Wang, X. Y.; Wang, L.; Wang, Z. M.; Su, G.; Gao, S. Coexistence of Spin-Canting, Metamagnetism, and Spin-Flop in a (4, 4) Layered Manganese Azide Polymer. *Chem. Mater.* **2005**, *17*, 6369−6380.

(29) Tomioka, Y.; Asamitsu, A.; Kuwahara, H.; Moritomo, Y.; Tokura, Y. Magnetic-Field-Induced Metal-Insulator Phenomena in $Pr_{1-x}Ca_xMnO_3$ with Controlled Charge-Ordering Instability. *Phys. Rev. B: Condens. Matter Mater. Phys.* **1996**, *53*, R1689.

(30) Gibson, Q. D.; Wu, H.; Liang, T.; Ali, M. N.; Ong, N. P.; Huang, Q.; Cava, R. J. Magnetic and Electronic Properties of $CaMn_2Bi_2$: A Possible Hybridization Gap Semiconductor. *Phys. Rev. B: Condens. Matter Mater. Phys.* **2015**, *91*, 085128.

(31) Kawaguchi, N.; Urata, T.; Hatano, T.; Iida, K.; Ikuta, H. Nonmonotonic and Anisotropic Magnetoresistance Effect in Antiferromagnet $CaMn_2Bi_2$. *Phys. Rev. B: Condens. Matter Mater. Phys.* **2018**, *97*, 140403.

(32) Cordier, G.; Schäfer, H. Neue Intermetallische Verbindungen Im Anti-Ce_2O_2S-Strukturtyp. /New Intermetallic Compounds in the Anti-Ce_2O_2S-Structure Type. *Z. Naturforsch. B* **1976**, *31*, 1459−1461.

(33) Singh, Y.; Gegenwart, P. Antiferromagnetic Mott Insulating State in Single Crystals of the Honeycomb Lattice Material Na_2IrO_3. *Phys. Rev. B: Condens. Matter Mater. Phys.* **2010**, *82*, 064412.

(34) Sears, J. A.; Songvilay, M.; Plumb, K. W.; Clancy, J. P.; Qiu, Y.; Zhao, Y.; Parshall, D.; Kim, Y. J. Magnetic Order in α−$RuCl_3$: A Honeycomb-Lattice Quantum Magnet with Strong Spin-Orbit Coupling. *Phys. Rev. B: Condens. Matter Mater. Phys.* **2015**, *91*, 144420.

(35) Matsuda, M.; Azuma, M.; Tokunaga, M.; Shimakawa, Y.; Kumada, N. Disordered Ground State and Magnetic Field-Induced Long-Range Order in an S= 3/2 Antiferromagnetic Honeycomb Lattice Compound $Bi_3Mn_4O_{12}(NO_3)$. *Phys. Rev. Lett.* **2010**, *105*, 187201.

(36) Zhang, A.; Liu, C.; Yi, C.; Zhao, G.; Xia, T.; Ji, J.; Shi, Y.; Yu, R.; Wang, X.; Chen, C.; et al. Interplay of Dirac Electrons and Magnetism in $CaMnBi_2$ and $SrMnBi_2$. *Nat. Commun.* **2016**, *7*, 13833.

(37) Park, J.; Lee, G.; Wolff-Fabris, F.; Koh, Y. Y.; Eom, M. J.; Kim, Y. K.; Farhan, M. A.; Jo, Y. J.; Kim, C.; Shim, J. H.; Kim, J. S. Anisotropic Dirac Fermions in a Bi Square Net of $SrMnBi_2$. *Phys. Rev. Lett.* **2011**, *107*, 126402.

(38) Chaudhuri, D.; Cheng, B.; Yaresko, A.; Gibson, Q. D.; Cava, R. J.; Armitage, N. P. Optical Investigation of the Strong Spin-Orbit-Coupled Magnetic Semimetal $YMnBi_2$. *Phys. Rev. B: Condens. Matter Mater. Phys.* **2017**, *96*, 075151.

(39) McMillan, P. F. New Materials from High-Pressure Experiments. *Nat. Mater.* **2002**, *1*, 19−25.

(40) Walsh, J. P. S.; Freedman, D. E. High-Pressure Synthesis: A New Frontier in the Search for Next-Generation Intermetallic Compounds. *Acc. Chem. Res.* **2018**, *51*, 1315−1323.

DOI: 10.1021/acs.inorgchem.9b01362
Inorg. Chem. 2019, 58, 8933−8937

(41) Badding, J. V. High-Pressure Synthesis, Characterization, and Tuning of Solid State Materials. *Annu. Rev. Mater. Sci.* **1998**, *28*, 631−658.
(42) Zhang, S. B.; Cohen, M. L. High-Pressure Phases of III-V Zinc-Blende Semiconductors. *Phys. Rev. B: Condens. Matter Mater. Phys.* **1987**, *35*, 7604−7610.
(43) Ying, J.-J.; Struzhkin, V. V.; Cao, Z.-Y.; Goncharov, A. F.; Mao, H.-K.; Chen, F.; Chen, X.-H.; Gavriliuk, A. G.; Chen, X.-J. Realization of Insulating State and Superconductivity in the Rashba Semiconductor BiTeCl. *Phys. Rev. B: Condens. Matter Mater. Phys.* **2016**, *93*, 100504.
(44) Hegger, H.; Petrovic, C.; Moshopoulou, E. G.; Hundley, M. F.; Sarrao, J. L.; Fisk, Z.; Thompson, J. D. Pressure-Induced Superconductivity in Quasi-2D $CeRhIn_5$. *Phys. Rev. Lett.* **2000**, *84*, 4986.
(45) Torikachvili, M. S.; Bud'ko, S. L.; Ni, N.; Canfield, P. C. Pressure Induced Superconductivity in $CaFe_2As_2$. *Phys. Rev. Lett.* **2008**, *101*, 057006.
(46) Takahashi, H.; Sugimoto, A.; Nambu, Y.; Yamauchi, T.; Hirata, Y.; Kawakami, T.; Avdeev, M.; Matsubayashi, K.; Du, F.; Kawashima, C.; Soeda, H.; et al. Pressure-Induced Superconductivity in the Iron-Based Ladder Material $BaFe_2S_3$. *Nat. Mater.* **2015**, *14*, 1008.
(47) Wu, M. K.; Ashburn, J. R.; Torng, C.; Hor, P. H.; Meng, R. L.; Gao, L.; Huang, Z. J.; Wang, Y. Q.; Chu, A. Superconductivity at 93 K in a New Mixed-Phase Y-Ba-Cu-O Compound System at Ambient Pressure. *Phys. Rev. Lett.* **1987**, *58*, 908.
(48) Sun, L.; Chen, X. J.; Guo, J.; Gao, P.; Huang, Q. Z.; Wang, H.; Fang, M.; Chen, X.; Chen, G.; Wu, Q.; Zhang, C.; et al. Re-Emerging Superconductivity at 48 K in Iron Chalcogenides. *Nature* **2012**, *483*, 67.
(49) Struzhkin, V. V.; Eremets, M. I.; Gan, W.; Mao, H. K.; Hemley, R. J. Superconductivity in Dense Lithium. *Science* **2002**, *298*, 1213−1215.
(50) Eremets, M. I.; Struzhkin, V. V.; Mao, H. K.; Hemley, R. J. Superconductivity in Boron. *Science* **2001**, *293*, 272−274.
(51) Somayazulu, M.; Ahart, M.; Mishra, A. K.; Geballe, Z. M.; Baldini, M.; Meng, Y.; Struzhkin, V. V.; Hemley, R. J. Evidence for Superconductivity above 260 K in Lanthanum Superhydride at Megabar Pressures. *Phys. Rev. Lett.* **2019**, *122*, 027001.
(52) Poirier, J.-P.; Tarantola, A. A Logarithmic Equation of State. *Phys. Earth Planet. Inter.* **1998**, *109*, 1−8.

DOI: 10.1021/acs.inorgchem.9b01362
Inorg. Chem. 2019, 58, 8933−8937